*EVS30 Symposium*
*Stuttgart, Germany, October 9 - 11, 2017*

# Coupled Energy-Saving and Safe-Driving Strategy for an Electric Vehicle Driven by Multiple Motors

Yee-Pien Yang[1, 2] and Wu-Chi Chen[1]

[1]*Department of Mechanical Engineering, National Taiwan University, Taipei, Taiwan*

[2]*Mechanical and Mechatronics Systems Research Laboratories, Industrial Technology Research Institute, Taiwan*

*ypyang@ntu.edu.tw*

**Abstract**

This paper proposes a coupled parallel energy-saving and safety strategy for an electric vehicle driven by multiple traction motors. Their torque distribution is determined by particle swarm optimization theory for minimizing energy consumption according to the torque-speed-efficiency maps of all the traction motors. Simultaneously, the torque distribution minimizes a stabilizing direct yaw moment according to the stability region on the yaw-rate and sideslip-angle phase plane. Experimental results on a hardware-in-the-loop platform show that the proposed strategy saves more energy than a serial energy-saving and driving-safety strategy that puts heavier emphasis on safe driving than energy saving.

*Keywords: electric vehicle, energy consumption, hardware-in-the-loop, optimization.*

## 1 Introduction

With the development of hub motors, the multi-motor configuration of electric vehicles (EVs) has been widely studied, including the rear in-wheel-motor drives [1, 2] and all in-wheel-motor drives [3, 4]. Both fuel economy and driving safety are considered, but they are usually in conflict with each other.

A few studies have focused on the objective of fuel economy of multi-motor EVs, where the torque split algorithm was used to minimize the total energy consumption of the vehicle. Wang et al. [5] investigated the energy-efficiency characteristics of an EV actuated by four in-wheel motors by their torque response and power-efficiency maps in both driving and regenerative braking modes. Yuan and Wang [6] proposed an online optimal torque distribution strategy to improve the drive train efficiency over a wide torque and speed range, where one of two identical motors was responsible for driving in the low-torque region and two of them for driving together in the remaining region. The drive train efficiency was improved by 4% over the New European Driving Cycle (NEDC) by experiments. Fujimoto and Harada [7] proposed a model-based range extension control system for an EV driven by four in-wheel motors, where the tire slip ratio and motor loss were optimized according to vehicle velocity and acceleration over the Japanese JC08 Cycle.

In addition to the fuel economy, some researchers focused on the driving safety of multi-motor EVs. Much research has been devoted to EVs driven by four independent in-wheel motors, among which the differential torque was usually determined for stabilizing the vehicle by a torque split algorithm [8-13]. Wu et al. [8] and Chen and Kuo [9] proposed an optimal wheel force distribution among four in-wheel motors on the EV by

minimizing the tire adhesion utilization rate based on the direct yaw-moment control (DYC). The coordination control of the hydraulic braking and the motor braking torque were also considered, and the vehicle stability was improved by simulations and experiments. Mirzaeinejad and Mirzaei [10] found that the existence of a direct yaw moment makes the stopping distance longer. They proposed an optimal nonlinear algorithm for distribution of tire braking forces to get a trade-off between the shorter stopping distance and less lane deviation. Jalali et al. [11] investigated an integrated approach of an advanced slip control, a torque vectoring control, and a genetic fuzzy active steering control to distribute the required control effort between the in-wheel motors and the active steering system. Li et al. [12] proposed an integrated control algorithm of active front steering (AFS) and DYC based on model prediction control. Shuai et al. [13] combined AFS and DYC control of four-wheel-independent-drive electric vehicles over the controller area network (CAN) bus with time-varying delays.

However, the objectives of fuel economy and driving safety are in conflict with each other. The DYC system uses a left-and-right-wheel differential torque to stabilize the vehicle, but when left and right hub motors are identical, they cannot simultaneously be operated in a high-efficiency torque region because of the existence of that differential torque. The conventional strategy does not consider the conflict, so both two mentioned objectives are integrated merely by pure series connection, named a "series energy-saving and safety" (SES) strategy. Hence, in this paper, a "parallel energy-saving and safety" (PES) strategy is proposed. PES is a strategy that minimizes the direct yaw moment when the vehicle is safely driven. Phase plane analysis is an effective way to examine vehicle stability [14–16]. In this paper, based on the result of phase plane analysis, a trade-off between maintaining and minimizing the direct yaw moment is determined.

# 2 Vehicle Models

## 2.1 Vehicle Specifications

The electric vehicle is installed with a 15-kW radial-flux permanent magnet synchronous motor (PMSM) to drive two front wheels indirectly with a gearbox reducer, and two identical 7-kW axial-flux PMSMs to drive two rear wheels directly through hubs, as shown in Fig. 1. Their torque, speed, and efficiency (TNE) maps given by experiments are shown in Fig. 2(a)(b) for the driving modes of the traction motors, while their braking modes in Fig. 2(c)(d) are estimated from the mirror image of 75% efficiency of the driving mode. Three motor control units are used to drive the 15-kW and 7-kW motors, and three lithium-ion batteries act as power sources, including one 144-V and two 72-V packages.

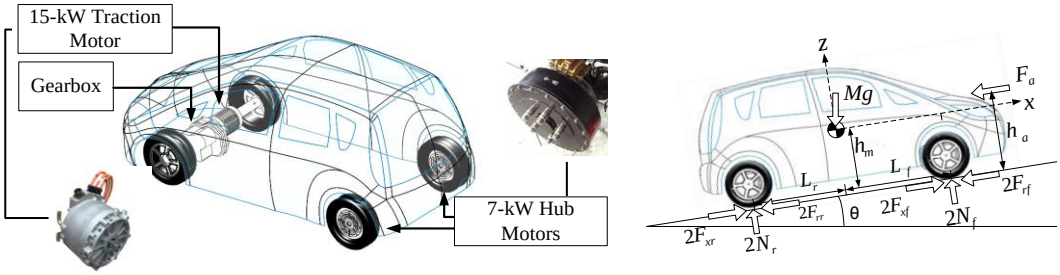


Figure 1: (a) Powertrain configuration of EV, and (b) definition of variables.

The simulation software CarSim is used to validate the control strategy for the four-wheeled vehicle with 15 mechanical degrees of freedom (DOF) [17]. The sprung mass is a rigid body with six DOF, each suspension has two DOF, each wheel has one spin DOF, and the steering system has one DOF. The specifications of the EV and its traction motors are given in Table 1. The CarSim tire look-up table obtained directly from laboratory measurement is used to model the tire characteristics.

## 2.2 Longitudinal Vehicle Dynamics Model

The longitudinal dynamics model of the vehicle is generated with variables and parameters introduced in Fig. 1(b). The normal forces $N_f$ and $N_r$ of the front and rear wheels and the tractive force $F_x$ are obtained by the following equations:

$$N_f = \left(Mg\cos\theta - \frac{1}{2}\rho C_d A_f V_x^2 h_a - Mh_m\dot{V}_x\right)/2(L_f + L_r) \quad (1)$$

$$N_r = \left(Mg\cos\theta + \frac{1}{2}\rho C_d A_f V_x^2 h_a + Mh_m\dot{V}_x\right)/2(L_f + L_r) \quad (2)$$

$$F_x = 2(F_{xf} + F_{xr}) = M\dot{V}_x + Mg\sin\theta + \frac{1}{2}\rho C_d A_f V_x^2 + 2C_r(N_f + N_r) \quad (3)$$

where $M$ is the vehicle mass; $\rho$ is the air density; $C_d$ is the aerodynamic coefficient; $C_r$ is the rolling resistance between tire and ground; $A_f$ is the frontal area of the vehicle; $V_x$ is the longitudinal speed of velocity; $h_m$ is the height of the mass centre; $h_a$ is the height of the equivalent aerodynamic point; $L_f$ and $L_r$ are the longitudinal distances from the mass centre to the ground points of the front and rear tires, respectively; and $F_{xf}$ and $F_{xr}$ are the traction force exerted on the front and rear tires, respectively.

The total torque $T_t$ used to accelerate the vehicle is

$$T_t = (F_x/r_t) = T_{mf}n_g + T_{mr} + T_{ml} \quad (4)$$

where $r_t$ is the tire radius, $T_{mf}$ is the torque provided by the front traction motor, $T_{mr}$ is the torque provided by the right rear in-wheel motor, and $T_{ml}$ is the torque provided by the left rear in-wheel motor.

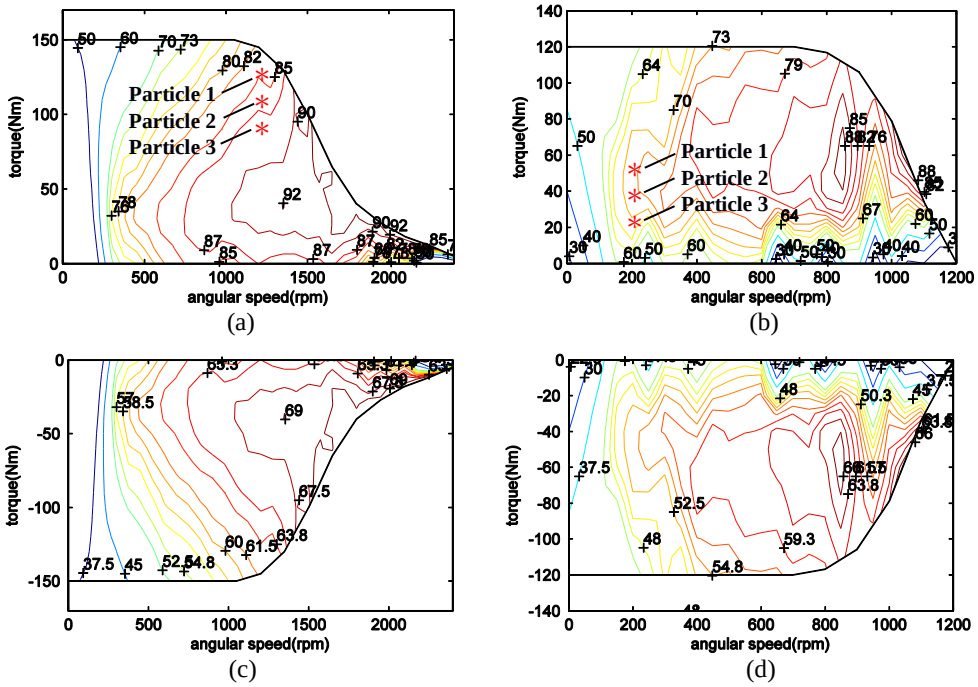


Figure 2: Torque-speed-efficiency maps of (a) the driving mode of the 15-kW motor, (b) the driving mode of the 7-kW motor, (c) the braking mode of the 15-kW motor, and (d) the braking mode of the 7-kW motor.

## 2.3 Lateral Vehicle Dynamics Model

A simplified bicycle model is used to describe the lateral vehicle dynamics and generate a stability region on the yaw-rate and sideslip-angle phase plane, which provides a boundary of torque distribution that minimizes a stabilizing direct yaw moment. As shown in Fig. 3, when the front wheel steer angle δ is small, the governing equations of the simplified vehicle model are

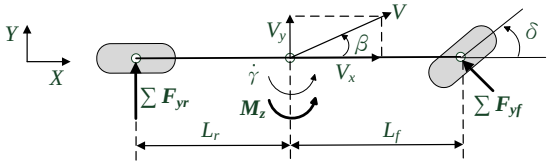


Figure 3: Bicycle model of the vehicle.

$$Ma_y = MV_x\left(\frac{\mathrm{d}}{\mathrm{d}t}\beta + \gamma\right) = 2F_{yf} + 2F_{yr} \tag{5}$$

$$I_z\dot{\gamma} = 2L_fF_{yf} - 2L_rF_{yr} + M_z \tag{6}$$

$$M_z = \frac{L_w}{2}\left(F_{xfr} - F_{xfl}\right) + \frac{L_w}{2}\left(F_{xrr} - F_{xrl}\right) \tag{7}$$

where $a_y$ is the vehicle lateral acceleration; $\beta$ is the vehicle sideslip angle; $\gamma$ is the vehicle yaw rate; $F_{yf}$ and $F_{yr}$ respectively stand for the lateral force on the front and rear tires; $I_z$ is the moment of inertia of the vehicle in the yaw direction; $L_f$ and $L_r$ are the distance from the center of gravity of the vehicle to the front and rear wheel axles, respectively; $M_z$ is the direct yaw moment generated by differential longitudinal tire forces; $F_{xfr}$ and $F_{xfl}$ are the longitudinal force on the right and left front tires, respectively; $F_{xrr}$ and $F_{xrl}$ are the longitudinal force on the right and left rear tires, respectively; $L_w$ is the distance between the left and right wheels.

Table 1: Specifications of the vehicle and traction motors

| Vehicle | Symbol | Value |
|---|---|---|
| Frontal area of vehicle | $A_f$ | 1.6 m$^2$ |
| Aerodynamic coefficient | $C_d$ | 0.28 |
| Rolling resistance between tire and ground | $C_r$ | 0.01 |
| Height of equivalent aerodynamic point | $h_a$ | 1 m |
| Height of mass center | $h_m$ | 0.56 m |
| Distance from mass center to front tire | $L_f$ | 1.433 m |
| Distance from mass center to rear tire | $L_r$ | 1.067 m |
| Distance between two rear wheels | $L_w$ | 1.46 m |
| Total mass of vehicle | $M$ | 1813 kg |
| Sprung mass of vehicle | $M_s$ | 1753 kg |
| Yaw inertia of vehicle | $I_z$ | 1200 kg·m$^2$ |
| Tire radius | $r_t$ | 0.288 m |
| Gear ratio | $n_g$ | 3 |
| Traction motors | 15-kW BLDC traction motor | 7-kW PMSM in-wheel motors |
| Flux type | Radial flux | Axial flux |
| Max. torque | 150 N·m | 122 N·m |
| Speed range | 0~2400 rpm | 0~1200 rpm |

For a small tire-slip angle, the lateral tire forces can be represented by functions of the constant cornering stiffness of the tires, as follows:

$$F_{yf} = -C_f\alpha_f = -C_f\left(\beta + \frac{\gamma L_f}{V_x} - \delta\right) \tag{8}$$

$$F_{yr} = -C_r\alpha_r = -C_r\left(\beta - \frac{\gamma L_r}{V_x}\right) \tag{9}$$

Hence, the governing equations of motion can be further transformed into the following linear-state space equation:

$$\begin{bmatrix}\frac{\mathrm{d}}{\mathrm{d}t}\beta \\ \frac{\mathrm{d}}{\mathrm{d}t}\gamma\end{bmatrix} = \begin{bmatrix}\frac{-(2C_f + 2C_r)}{MV_x} & \frac{-2L_fC_f + 2L_rC_r}{MV_x^2} - 1 \\ \frac{-2L_fC_f + 2L_rC_r}{I_z} & \frac{-2L_f^2C_f - 2L_r^2C_r}{I_zV_x}\end{bmatrix}\begin{bmatrix}\beta \\ \gamma\end{bmatrix} + \begin{bmatrix}\frac{2C_f}{MV_x} & 0 \\ \frac{2L_fC_f}{I_z} & \frac{1}{I_z}\end{bmatrix}\begin{bmatrix}\delta \\ M_z\end{bmatrix} \tag{10}$$

where $V_x$ is the longitudinal velocity of the vehicle, and $C_f$ and $C_r$ are the cornering stiffness of the front and rear tires, respectively.

# 3 Parallel Energy-Saving and Safety (PES) Strategy

The DYC that uses the differential torque between the left- and right-wheel motors is proposed to stabilize the vehicle during severe maneuvers by tracking a yaw-rate command, which is the steady-state yaw rate obtained by (10):

$$\gamma^* = \frac{V_x \delta}{(L_f + L_r) + \frac{M(L_r C_r - L_f C_f) V_x^2}{2 C_f C_r (L_f + L_r)}} \tag{11}$$

The corresponding yaw moment $M_z$ in the steady state of a small steer angle is provided by the differential torque of the left and right in-wheel motors:

$$M_z = \frac{L_w}{2 r_t}(T_{mr} - T_{ml}) = \frac{L_w}{2 r_t}\Delta T_m \tag{12}$$

The existence of a direct yaw moment aims to stabilize the vehicle for driving safety, but it usually consumes much driving energy. To compromise between driving safety and energy saving, a sliding mode control (SMC) is employed. A sliding surface $S$ is formed by the direct yaw-moment magnitude and yaw-rate error, and is switched by a weighting factor $w_{sm}$:

$$S = (1 - w_{sm})(\gamma - \gamma^*) + \frac{w_{sm}}{I_z K} M_z, \tag{13}$$

where the control gain $K$ is obtained by the SMC law:

$$\dot{S} = (1 - w_{sm})(\dot{\gamma} - \dot{\gamma}^*) = -KS \tag{14}$$

Here, $\dot{\gamma}$ is the yaw acceleration and $\dot{\gamma}^*$ is the desired yaw acceleration. The weighting factor $w_{sm}$ is determined within [0, 1] by the yaw-rate and sideslip-angle ($\beta$–$\gamma$) phase plane, as shown in Fig. 4. The parallelogram region defines a stability boundary, where $\beta_{bd}$ represents the boundary of the sideslip angle and $\gamma_{bd}$ represents the boundary of the yaw rate.

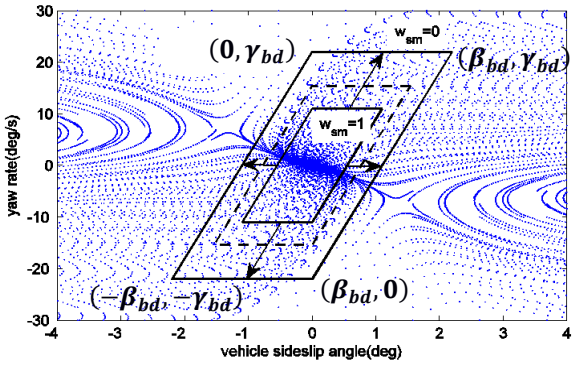


Figure 4: Stability region on the sideslip-angle and yaw-rate phase plane.

Therefore, the direct yaw-moment command becomes

$$M_z = (1 - w_{sm})\left[-I_z K(\gamma - \gamma^*) + \left(I_z \dot{\gamma}^* - 2L_f F_{yf} + 2L_r F_{yr}\right)\right] \tag{15}$$

The weighting factor $w_{sm}$ represents the compromise between driving safety and energy saving. A smaller $w_{sm}$ requires more power to produce a yaw moment for driving safely, while the energy saving is less important. A larger $w_{sm}$ results in more energy saving but less safe driving. According to the stability region on the $\beta$–$\gamma$ phase plane, the weighting factor is determined by $w_{sm} = min(w_1, w_2)$, where

$$w_1 = \begin{cases} \frac{\beta_{bd}/2 - \left|\beta - \frac{\beta_{bd}}{2\gamma_{bd}}\gamma\right|}{\beta_{bd}/4} & , \text{if } \frac{\beta_{bd}}{2} \le \left|\beta - \frac{\beta_{bd}}{2\gamma_{bd}}\gamma\right| \le \beta_{bd} \\ 0 & , \text{if } \frac{\beta_{bd}}{2} > \left|\beta - \frac{\beta_{bd}}{2\gamma_{bd}}\gamma\right| \\ 1 & , \text{if } \beta_{bd} < \left|\beta - \frac{\beta_{bd}}{2\gamma_{bd}}\gamma\right| \end{cases} \tag{16}$$

and

$$w_2 = \begin{cases} \frac{\gamma_{bd}-|\gamma|}{\gamma_{bd}/2} & ,\text{if } \frac{\gamma_{bd}}{2} \le |\gamma| \le \gamma_{bd} \\ 0 & ,\text{if } \frac{\gamma_{bd}}{2} > |\gamma| \\ 1 & ,\text{if } \beta_{bd} < |\gamma| \end{cases} \tag{17}$$

# 4 Experiments

The torque distribution among the three traction motors is determined by simultaneously weighing up the importance of energy saving compared with driving safety. For energy saving, the torque distribution is determined by particle swarm optimization (PSO) theory for minimizing energy consumption according to the torque-speed-efficiency maps of all the traction motors. Simultaneously, the torque distribution minimizes a stabilizing direct yaw moment according to the stability region on the yaw-rate and sideslip-angle phase plane. The sliding mode control (SMC) is employed to design the direct yaw-moment controller. The coupled energy-saving and safe-driving control structure is illustrated in a hardware-in-the-loop (HIL) platform, as shown in Fig. 5, which consists of an RT-LAB, MicroAutoBox II, and dynamometer. All the HIL equipment communicates via the control area network (CAN) bus.

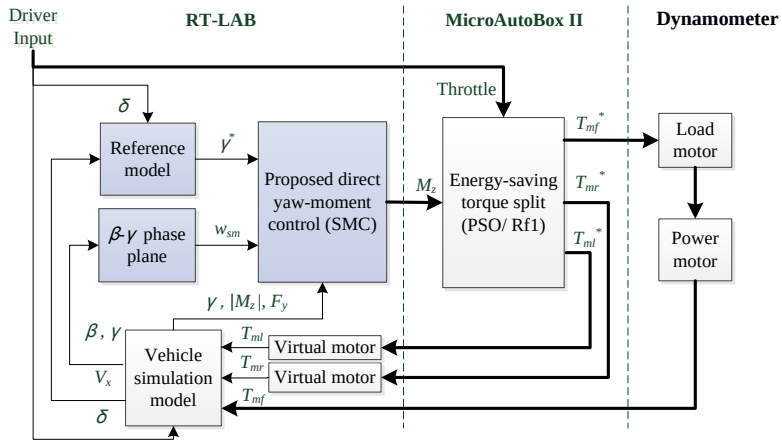


Figure 5: HIL architecture of coupled energy-saving and safe-driving strategy.

The two virtual motors simulated the dynamics of the 7-kW in-wheel motors; the real traction motor acted as the 15-kW traction motor for the EV. The EV was modeled by the software CarSim, the direct yaw-moment controller was built with Matlab/Simulink, and both were compiled by RT-Lab. A look-up table of tire parameters obtained by laboratory measurement was built with CarSim, and a plot of tire lateral force versus slip angle for different vertical tire loads is given in Fig. 6.

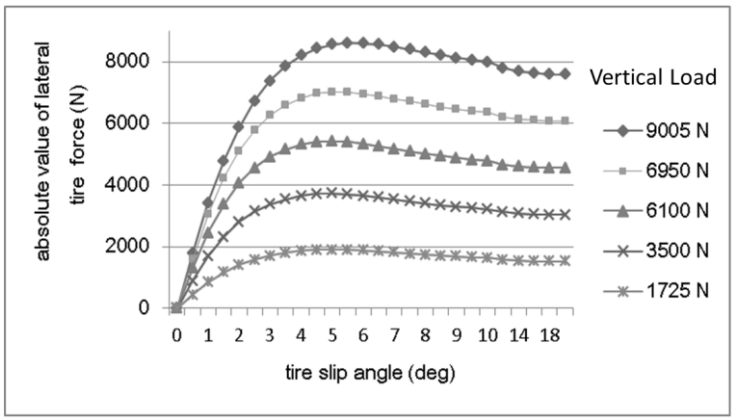


Figure 6: Tire model of lateral force and slip angle.

## 4.1 Double-Lane Change Test

Driving safety was examined through a double-lane change test. The test driving path followed the ISO 3888-2 standard, as shown in Fig. 7. The initial vehicle velocity was 20 km/h, the road friction coefficient was 0.4, and the driver applied 60% throttle to drive the EV. The proposed parallel energy-saving and driving-safety (PES) strategy examined the current stability status on the $\beta$–$\gamma$ phase plane. The sliding-mode-surface weighting factor $w_{sm}$ in (15)–(17) was tuned between 0 and 1, as a compromise between energy saving and driving safety. For the extreme case of $w_{sm} = 0$ when the vehicle is on the boundary of instability, more power is taken to produce a yaw moment to guarantee safe driving, but less importance is attached to energy saving. This is called the "serial energy-saving and driving strategy" (SES). When the direct yaw-moment control is not applied as $M_z = 0$, only the energy-saving strategy is executed.

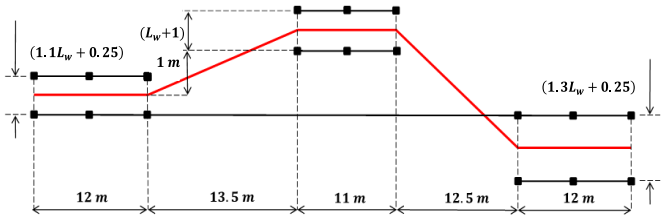


Figure 7: Double-lane change of driving path in ISO 3888-2.

Fig. 8(a) illustrates the direct yaw-moment histories during the double-lane change, where the SES takes more power to produce a larger yaw moment for safe driving. Fig. 8(b) shows the weighting factor for the PES strategy during the maneuver test. Both the yaw rates of the PES and SES control strategies follow the desired yaw rate for driving safety, as shown in Fig. 8(c), and the vehicle performs well on the double-lane change path in Fig. 8(d). When the direct yaw-moment control is not applied ($M_z = 0$), the vehicle deviates away from the path, which is indicated as the "no control" status in the figures.

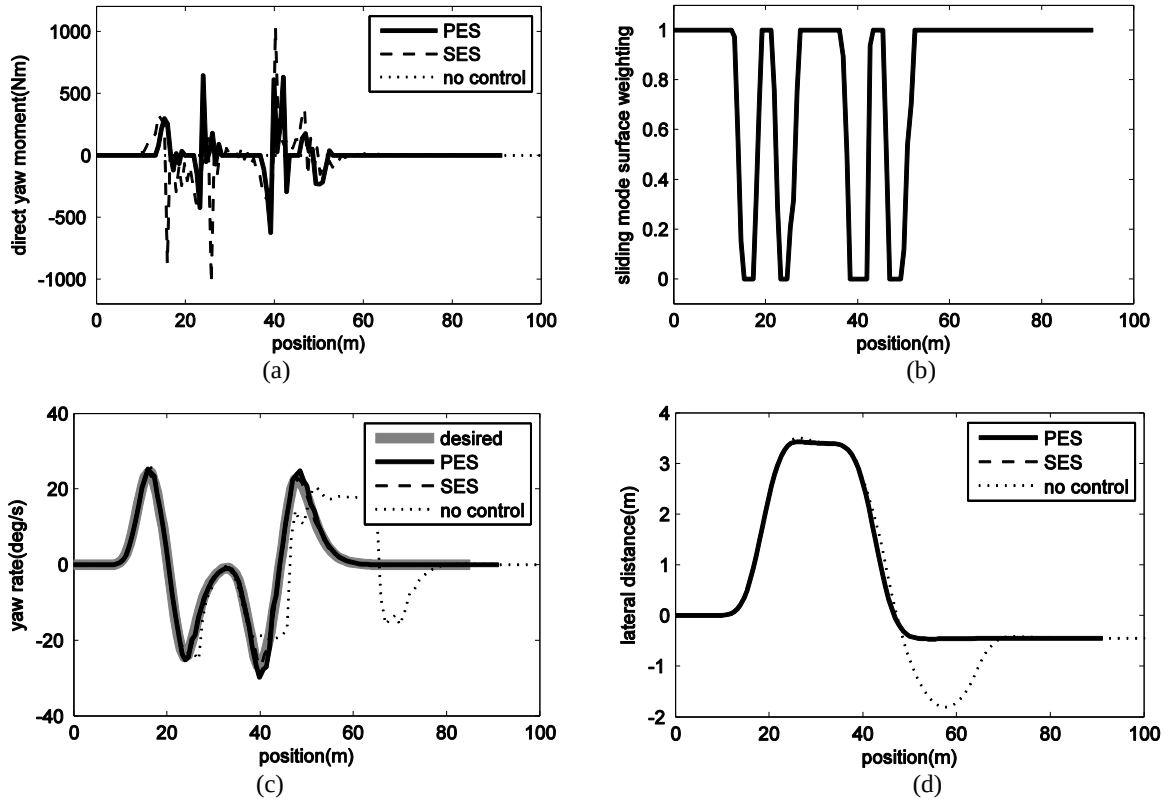


Figure 8: Results of double-lane change test: (a) direct yaw-moment histories, (b) sliding-mode-surface weighting of the PES strategy, (c) yaw rates, and (d) driving trajectories.

## 4.2 Urban Driving Cycle Test

The energy-saving ability during vehicle cornering was examined on a circular path to follow the urban driving cycle (UDC) schedule, as shown in Fig. 9. The simulation time was 820 s, the corresponding driving range was 3.97 km, and the maximum vehicle speed was 50 km/h. The total torque command from driver $T_{total}$ is achieved by the output torque of the front motor $T_{mf}$, the output torque of the left rear motor $T_{ml}$, and the output torque of the right rear motor $T_{mr}$. Their relationship is expressed as (4).

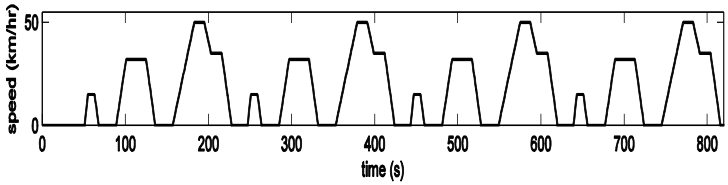


Figure 9: The urban driving cycle (UDC).

To decide the output torque of each motor, the direct yaw-moment command $M_z$, the maximum torque of each motor, and the angular speed of each motor $\omega_{mf}$, $\omega_{ml}$, and $\omega_{mr}$ should be given. The minimum and maximum allowable output torques of the front motor $T_{allow,min}$ and $T_{allow,max}$ can be calculated, so that an allowable output range of the front motor is obtained. Between $T_{allow,min}$ and $T_{allow,max}$, $T_{mf}$ is determined by the particle swarm optimization (PSO) algorithm.

The particle swarm optimization (PSO) theory originated from the observation of the hunting behaviour of a swarm of fish or birds. In the torque distribution process, a particle is a point on a TNE map, which is known as a search space. Initially, three swarms of particles are distributed randomly on the three TNE maps of traction motors, two of them as shown in Fig. 1(a)(b). Each swarm on each map has $N$ particles. The position state of each particle is defined as the torque where the particle is located. The common target is the throttle command given by the driver of the EV.

Each individual recognized as a particle, at its initial position in a search space, determines its best direction and all the particles approach their common target with the minimal global effort.

$$J = \frac{T_{mf}\omega_{mf}}{\eta_{mf}(T_{mf},\omega_{mf})} + \frac{T_{ml}\omega_{ml}}{\eta_{ml}(T_{ml},\omega_{ml})} + \frac{T_{mr}\omega_{mr}}{\eta_{mr}(T_{mr},\omega_{mr})} \tag{18}$$

The lower limit and upper limit of the torque produced by the front traction motor and two rear motors are determined by (4), (12)–(16), and the battery capacity. During the PSO process, the $N$ particles will be renewed through $J$ generations, and finally all reach the target of minimal energy consumption. For each generation, the least energy consumption converges, and particles are updated according to own best and swarm best solution as

$$\Delta T_{mf,i}^{j+1} = wT_{mf,i}^{j+1} + rand_1 \times c_{L1}\left(P_i^j - T_{mf,i}^j\right) + rand_2 \times c_{L2}\left(G^j - T_{mf,i}^j\right) \tag{19}$$

$$T_{mf,i}^{j+1} = T_{mf,i}^j + \Delta T_{mf,i}^{j+1} \tag{20}$$

until the final generation is achieved, where the sub-index $i$ stands for the $i^{th}$ particle; $j$ stands for the generation number; $w$ is the inertia weight; $c_{L1}$ and $c_{L2}$ are learning factors; $rand_1$ and $rand_2$ are random values between 0 and 1; $P_i$ represents the own best-known solution of the $i^{th}$ particle; and $G$ represents the swarm best-known solution of all particles. The output torques of rear motors are then calculated by the following equations

$$T_{ml} = \frac{T_{total} - T_{mf} \times n_g}{2} - \frac{r_t M_z}{L_w} \tag{21}$$

$$T_{mr} = \frac{T_{total} - T_{mf} \times n_g}{2} + \frac{r_t M_z}{L_w} \tag{22}$$

The directional stability is guaranteed by applying the yaw moment $M_z$, which is generated by the differential torque between the left and right hub motors by (12). However, there is a conflict between the objectives of energy saving and driving safety. Here, both the PES and SES strategies are investigated for the EV moves

on a circular path of radius 60 m to demonstrate the torque split performance, as shown in Fig. 10.

It is found that the weighting factor $w_{sm}$ and the yaw moment $M_z$ are tuned when the PES strategy is implemented. The differential torque between the left and right rear hub motors is minimized, and the front traction motor, which is more efficient than the rear motors, is responsible for producing more torque. Table 2 shows the energy consumption from more experiments for the EV cornering along circular paths of various radii. The proposed PES strategy consumes 1–4.6% less energy than the SES strategy.

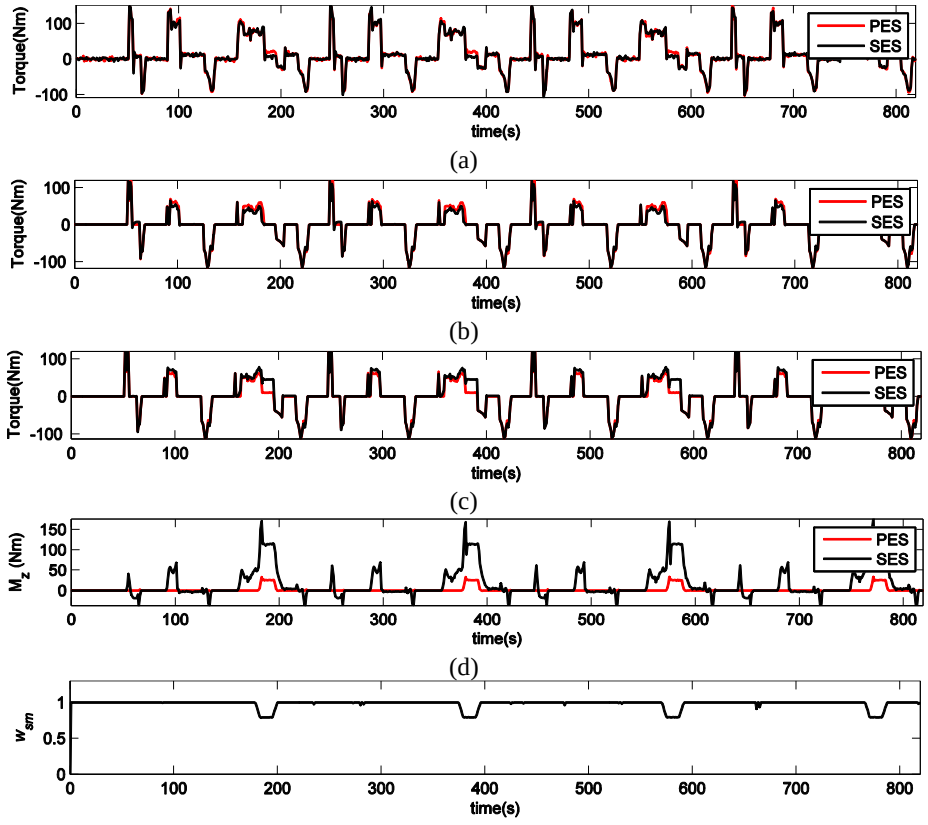


Figure 10: Torque split histories for the EV moving along a circular path of radius of 60 m by the parallel and serial energy-saving and driving-safety control strategies: torques produced by (a) the front traction motor, (b) the left rear hub motor, and (c) the right rear hub motor; (d) the direct yaw moments; and (e) the weighting factor for the PES strategy.

Table 2: Energy consumption during EV cornering by the PES and SES strategies, based on the PSO algorithm

| Path radius | Strategy | Energy consumption and saving ratio | |
|---|---|---|---|
| | | Watt-hours (Wh) | % |
| 100 m | PES | 415.94 | 1.4% |
| | SES | 421.98 | - |
| 80 m | PES | 420.00 | 1.4% |
| | SES | 425.93 | - |
| 60 m | PES | 438.03 | 1.0% |
| | SES | 442.41 | - |
| 40 m | PES | 514.76 | 4.6% |
| | SES | 539.42 | - |

## 5. Conclusions

This research has proposed a parallel energy-saving and safety-control strategy based on particle swarm optimization for an EV driven by multiple motors. The stabilizing yaw moment is minimized for driving the EV within the stability region in the yaw-rate and sideslip-angle ($\beta$–$\gamma$) phase plane. The proposed PES strategy is validated by the HIL platform, and the experimental results show that the parallel energy-saving and safety-control

strategy is able to stabilize the EV during severe maneuvers. Also, the PES control strategy saves 1%~4.6% more energy than the serial energy-saving and driving-safety control strategy, which puts more emphasis on driving safety than on energy saving. The proposed parallel energy-saving and safety-control strategy will be implemented on an EV with three traction motors, and both energy saving and safety driving for the EV will be realized in road tests in the future.

## Acknowledgments

This work was supported by Ministry of Science and Technology, Taiwan, Republic of China under grant number MOST 104-2221-E-002-087-MY2.

## References

[1] K. Nam, S. Oh, and H. Fujimoto, *robust yaw stability control for electric vehicles based on active front steering control through a steer-by-wire system*, International Journal of Automotive Technology, 13(7), 1169-1176, 2012

[2] J. S. Hu, D. J. Yin, and Y. Hori, *fault-tolerant traction control of electric vehicles*, Control Engineering Practice, 19(2), 204-213, 2011

[3] B. Y. Li, H. P. Du, and W. H. Li, *fault-tolerant control of electric vehicles with in-wheel motors using actuator-grouping sliding mode controllers*, Mechanical Systems and Signal Processing, 72-73, 462-485, 2016

[4] P. Song, M. Tomizuka, and C. F. Zong, *a novel integrated chassis controller for full drive-by-wire vehicles*, Vehicle System Dynamics, 53(2), 215-236, 2015

[5] R. O. Wang, Y. Chen, D. W. Feng, X. Y. Huang, and J. M. Wang, *development and performance characterization of an electric ground vehicle with independently actuated in-wheel motors*, Journal of Power Sources, 196(8), 3962-3971, 2011

[6] X. B. Yuan and J. B. Wang, *torque distribution strategy for a front-and-rear-wheel-driven electric vehicle*, IEEE Transactions on Vehicular Technology, 61(8), 3365-3374, 2012

[7] H. Fujimoto and S. Harada, *model-based range extension control system for electric vehicles with front and rear driving–braking force distributions*, IEEE Transactions on Industrial Electronics, 62(5), 3245-3254, 2015

[8] D. M. Wu, H. T. Ding, K. H. Guo, Y. Sun, and Y. Li, *stability control of four-wheel-drive electric vehicle with electro-hydraulic braking system*, SAE Technical Paper, 2014-01-2539, 2014

[9] B. C. Chen and C. C. Kuo, electronic stability control for electric vehicle with four in-wheel motors, International Journal of Automotive Technology, 15(4), 573-580. 2014

[10] H. Mirzaeinejad and M. Mirzaei, *optimization of nonlinear control strategy for anti-lock braking system with improvement of vehicle directional stability on split-$\mu$ roads*, Transportation Research Part C: Emerging Technologies, 46, 1-15, 2014

[11] K. Jalali, T. Uchida, J. McPhee, and S. Lambert, *development of an integrated control strategy consisting of an advanced torque vectoring controller and a genetic fuzzy active steering controller*, SAE International Journal of Passenger Cars-Electronic and Electrical Systems, 6(), 222-240, 2013

[12] G. Li, W. Hong, and H. Liang, *four-wheel independently driven in-wheel motors electric vehicle AFS and DYC integrated control*, SAE Technical Paper, 2012-01-0258, 2012

[13] Z. B. Shuai, H. Zhang, J. Wang, J. Li, and M. Ouyang, *combined AFS and DYC control of four-wheel-independent-drive electric vehicles over CAN network with time-varying delays*, IEEE Transactions Vehicular Technology, 63(2), 591-602, 2014

[14] L. D. Novellis, A. Sorniotti, P. Gruber, J. Orus, J.-M. R. Fortun, J. Theunissen, and J. De Smet. *direct yaw moment control actuated through electric drivetrains and friction brakes: theoretical design and experimental assessment*, Mechatronics, 26, 11-15, 2015

[15] S. Azadi, M. Naghibian, and R. Kazemi, *adaptive integrated control design for vehicle dynamics using phase-plane analysis*, Journal of Mechanical Science and Technology, 29(6), 2477-2485, 2015

[16] M. Doumiati, O. Sename, L. Dugard, J.-J. Martinez-Molina, P. Gaspar, and Z. Szabo, *integrated vehicle dynamics control via coordination of active front steering and rear braking*, European Journal of Control, 19(2), 121-143, 2013

[17] J. G. Yi, J. L. Li, J. B. Lu, and Z. D. Liu, *on the stability and agility of aggressive vehicle maneuvers: a pendulum-turn maneuver example*, IEEE Transactions on Control Systems Technology, 20(3), 663-676, 2012

# Authors

Yee-Pien Yang received the B.S. and M.S. degrees in mechanical engineering from National Cheng Kung University, Tainan, Taiwan, in 1979 and 1981, respectively, and the Ph.D. degree in mechanical, aerospace, and nuclear engineering from the University of California, Los Angeles, CA, USA, in 1988. He is now a professor in the Department of Mechanical Engineering, National Taiwan University, leading the Electromechanical System Research Group at the Propulsion Control laboratory. He is also a Deputy General Director of the Mechanical and Mechatronics Systems Research Laboratories in the Industrial Technology Research Institute, conducting research on the electric vehicles, electric machines, and assistive tools for the disabled.

Wu-Chi Chen received the B.S. degree in mechanical engineering from Yuan Ze University, Taoyuan, Taiwan, in 2013, and M.S. degree in mechanical engineering from National Taiwan University, Taipei, Taiwan, in 2016. He is currently an automation engineering in Avary Holding Ltd., providing optimal motion program and solution for machines of production line. His areas of interests include optimization algorithm, vehicle dynamics, programming, and intelligence control.